Effect of resonant magnetic perturbations on local plasma current density gradients and neoclassical tearing modes

Q. Yu, S. Günter and K. Lackner*

Max-Planck-Institut für Plasmaphysik, 85748 Garching, Germany

Abstract: The effect of externally applied resonant magnetic perturbations (RMPs) on the local equilibrium plasma current density profile is studied numerically based on two-fluid equations in simplified cylindrical geometry. It is found that a moderate RMP below its penetration threshold, via non-linear mode coupling, induces a parallel electric field around its rational surface that can significantly change the local flux-surface-averaged current density gradient. At a given RMP amplitude, the modification of the current density profile increases with increasing electron temperature, and it significantly depends on the bi-normal electron fluid velocity at the resonant surface. The effect of this modification on the magnetic island growth is demonstrated by the example of small m/n=2/1 islands (m/n being the poloidal/toroidal mode numbers), driven by an unfavorable plasma current density profile and bootstrap current perturbation. The 2/1 mode growth is stabilized by moderate static 4/2 or 6/3 RMPs if the local electron fluid velocity is in the ion drift direction or sufficiently large in the electron drift direction. These results reveal that a weakly three-dimensional equilibrium, containing a moderate 4/2 RMP and the associated shielding current, can be more stable against the 2/1 mode, which often causes tokamak plasma major disruptions.

*e-mail: qingquan.yu@ipp.mpg.de

Key words: weakly three-dimensional equilibrium, resonant magnetic perturbation, error field, plasma current density gradient, magnetic island, neoclassical tearing mode, two-fluid physics

1. Introduction

Since the 1970s, externally applied resonant magnetic perturbations (RMPs) have attracted much interest in fusion research [1-15]. RMPs are found to have important effects on magnetic islands in tokamak plasmas. Sufficiently large RMPs can lock rotating magnetic islands or generate islands at their resonant surface even if the plasma was originally stable to tearing modes [1-15]. On the other hand, moderate $m/n = 2/1$ RMPs have been found to stabilize $2/1$ tearing modes in experiments [1-4,9], where $\mathrm{m/n}$ is the poloidal/toroidal mode number. Later, more research efforts have been devoted to understand the effect of RMPs on plasma rotation and density profile [16-21] and especially on mitigating or suppressing edge localized modes (ELMs) as is planned for ITER [22-32]. The penetration of $high - m$ RMPs in the pedestal region is found to cause the ELMs suppression and associated density pump-out in DIII-D experiments [31-32]. The density pump-out and the change of the local plasma rotation from the electron drift direction towards the ion's one are also often observed in ELMs suppression experiments by RMPs on ASDEX Upgrade and other tokamak [22-32], a two-fluid effect expected from theoretical results [18,20,21].

Recently the effect of the $m/n = 2/1$ RMPs on the growth of a $2/1$ magnetic island was studied numerically using two-fluid equations [33], including the electron diamagnetic drift and the associated ion polarization current, being important for the stability of a small magnetic island [34-41]. If the local bi-normal electron fluid velocity at the resonant surface was large enough, the growth of small $m/n = 2/1$ islands was found to be suppressed by static $2/1$ RMPs of moderate amplitude. In addition, the local flux-surface-averaged plasma current density gradient, i.e., the $m/n = 0/0$ component in cylinder geometry, has been found to be affected by the RMP at the $q = 2$ surface (q is the safety factor) [33].

The stability of MHD modes driven or partly driven by the current density gradient, such as the neoclassical tearing mode (NTM) and ELMs, strongly depends on the plasma current density profile around the resonant surface. It is therefore of great interest to understand the effect of RMPs on the local current density profile and its dependence on RMP amplitude and the plasma parameters. Even without applied RMPs, the error field can be in the order of 10^{-5} or 10^{-4} of the toroidal field in tokamaks, leading to the question that whether its amplitude is already large enough to affect the local current density profile.

In this paper the effect of externally applied $m/n = 4/2$ and $6/3$ RMPs on the local flux-surface-averaged plasma current density gradient is studied numerically, based on the four-field equations in a cylindrical plasma [42]. Two sets of plasma parameters, with an electron temperature of $T_e = 300eV$ (*high resistivity case*) and $T_e = 2keV$ (*low resistivity case*), are investigated,

respectively, in order to assess the dependence of the effect on plasma parameters. It is found that static $4/2$ or $6/3$ RMPs, via non-linear mode coupling, induce a parallel electric field at the $q = 2$ rational surface that can significantly change the local current density gradient, even at moderate RMP amplitude below the penetration threshold. The modification of the current density profile is already significant for the *high resistivity case*, and it increases with decreasing plasma resistivity. The current density profile modification is found to depend on the RMP amplitude, plasma rotation velocity, bootstrap current density, and other plasma parameters.

Based on the findings mentioned above, the effect of the $m/n = 4/2$ and $6/3$ RMPs on the growth of $2/1$ NTMs is further studied. The change in the local plasma current density by RMPs is found to significantly affect the NTM growth. In our test case without applied RMPs, a $m/n = 2/1$ magnetic island grows, driven by an unfavorable plasma current density profile and bootstrap current perturbation. The growth of a small $2/1$ island is affected by moderate $4/2$ or $6/3$ RMPs: the mode is stabilized if the bi-normal electron fluid velocity is in the ion drift direction or sufficiently large in the electron drift direction. Rotating RMPs in the electron drift direction with a frequency about the electron diamagnetic drift frequency are found to suppress the island growth even for zero electron fluid velocity, since only the relative rotation between the mode and RMPs counts. This differs from the effect of RMPs on the magnetic island of the same mode numbers [4,9,12,33], where RMPs can additionally cause a non-uniform island rotation and a change in the polarization current, both affecting the tearing mode stability. Our results reveal that a weakly three-dimensional equilibrium, containing a moderate $4/2$ or $6/3$ RMP and the associated shielding current, can be more stable against the $2/1$ mode, which is known to be a major cause for tokamak plasma major disruptions.

In the next section the analysis and numerical results for the change of the local plasma current density gradient of the $0/0$ component by RMPs are presented. The effects of the $m/n = 4/2$ and $6/3$ RMPs on the growth of the $2/1$ NTM are shown in Section 3 and compared to the effect of a $2/1$ RMP, followed by the discussion and summary in the last section.

2. Effect of RMPs on local plasma current density gradient

There are two mechanisms by which RMPs can cause the plasma current density of the $m/n = 0/0$ component, $j_{0/0}$, to differ from the original equilibrium one, j_0, around the resonant surface: (a) The nonlinearity from the parallel static electric field, electron pressure gradient and electron inertia in Ohm's law (see (A2) in the Appendix); (b) The change of the local plasma pressure gradient of the $m/n = 0/0$ component, which leads to a corresponding change in the local bootstrap and

plasma current density.

In order to find out the change of the equilibrium plasma current density, $\Delta j_{0/0} = (j_{0/0} - j_0)$, numerical calculations are generally required. In the following Section 2.1, a heuristic quasi-linear analysis will be carried out to find out the dependence of $\Delta j_{0/0}$ on plasma parameters in the framework of single fluid equations. Numerical calculation results based on the four-field equations [42], shown in the Appendix in the form of normalized units, will be presented in Section 2.2.

2.1 Heuristic quasilinear analysis

Assuming that the plasma is stable to a tearing mode with the mode numbers m/n, and the applied RMP of the same mode numbers is sufficiently small such that it has not penetrated in, it is found from the Ohm's law (equation (A2) in Appendix) that $\Delta j_{0/0}$ in steady state is determined by

$$2\eta_N(\Delta j_{0/0} - \Delta j_{b,0/0}) = [\boldsymbol{b_1}\cdot(\nabla f_1)^* + \boldsymbol{b}_1^*\cdot\nabla f_1] - (\frac{\eta_N}{\upsilon_{ei}})[\boldsymbol{v}_{E1}\cdot(\nabla j_1)^* + \boldsymbol{v}_{E1}^*\cdot\nabla j_1], \quad (1)$$

where $\eta_N = 1$ is the normalized plasma resistivity, $\Delta j_{b,0/0}$ is the change of the $0/0$ component of the bootstrap current density by RMPs from the original equilibrium one, the subscript 1 refers to a perturbed quantity of the m/n component driven by the RMP, the superscript $*$ is for the conjugated part, $\boldsymbol{b}$, $\boldsymbol{v}_E$ and j are the magnetic field, electric drift velocity and parallel plasma current density, respectively, and

$$f_1 = \phi_1 + \Omega_0 n_{e1}, \quad (2)$$

including the perturbations of the stream function ϕ_1 and electron density n_{e1}. $\Omega_0 = \Omega(T_{e0}/n_{e0})$, T_{e0} and n_{e0} are the equilibrium electron temperature and density, and the parameter Ω is a coefficient for the parallel electron pressure gradient in Ohm's law, defined in the Appendix. The last term in equation (1) is due to the electron inertia, and υ_{ei} is the normalized electron-ion collision frequency. All quantities in the above equations are in normalized units: The length is normalized to the plasma minor radius a, the time t to the resistive time $\tau_R = a^2\mu_0/\eta$ (η is the resistivity), $\boldsymbol{b}$ to the equilibrium toroidal field B_t, the current density to B_t/a, and the electron density n_e to its value at the magnetic axis.

When the electron inertia and bootstrap current density are neglected, equations (1) and (2) can be simplified to

$$\Delta j_{0/0} = 0.5ik_p(\psi_1 f_1^* - \psi_1^* f_1)'/\eta_N, \quad (3)$$

and it is found from Ohm's law of the m/n component that

$$ik_\parallel f_1 = i\omega_{e\perp N}\psi_1 + \eta_N j_1, \quad (4)$$

where i is the imaginary index, $k_p = m/r$, r is the minor radius, $k_\parallel$ is the parallel wave vector,

the prime stands for the radial gradient, $\omega_{e\perp N} = \omega_{e\perp}\tau_R = (\omega_{E0} + \omega_{*e0})\tau_R$ is the normalized bi-normal equilibrium electron fluid frequency, ω_{*e0} is the electron diamagnetic drift frequency, and ω_{E0} the electric drift frequency. The helical flux ψ is defined by $\boldsymbol{B} = B_t\boldsymbol{e}_t - \left(k_t/k_p\right)B_t\boldsymbol{e}_p + \nabla\psi \times \boldsymbol{e}_t$, where $k_t = n/R$, $\boldsymbol{e}_p$ ($\boldsymbol{e}_t$) is the unit vector in the poloidal (toroidal) direction, and R is the major radius. Equations (3) and (4) give the change in the equilibrium current density

$$\Delta j_{0/0} = -0.5k_p[(\psi_1 j_1^* + \psi_1^* j_1)/k_\parallel]', \tag{5}$$

which is caused by the plasma current density perturbation in phase with the magnetic island or ψ_1. It is worth to mention that the poloidal electromagnetic torque density of the $m/n = 0/0$ component is of a similar form [12,20],

$$T_{EM,p} = 0.5r(b_{1r}j_1^* + b_{1r}^* j_1) = -0.5im(\psi_1 j_1^* - \psi_1^* j_1), \tag{6}$$

but depends on the plasma current density perturbation having a $\pi/2$ phase difference with ψ_1. where the subscript r refers to the radial component. There is usually a phase shift between j_1 and ψ_1 around the resonant surface for rotating plasmas, depending on plasma parameters and rotation frequency [43].

In the following our analysis is limited to the framework of single fluid equations in steady state. In this case the Ohm's law and the plasma vorticity equation (equations (A2) and (A3) in the Appendix) become

$$\boldsymbol{v}_E \cdot \nabla\psi = E_0 - \eta_N j, \tag{7}$$

$$\boldsymbol{v}_E \cdot \nabla U = S^2\nabla_{||}j + \mu_N\nabla_\perp^2 U, \tag{8}$$

where $U = -\nabla_\perp^2\phi$ is the plasma vorticity, E_0 is the parallel equilibrium electric field, $S = \tau_R/\tau_A$, $\tau_A = a/V_A$ being the Alfven time, V_A is the Alfven velocity defined using the toroidal field, μ_N is the normalized plasma viscosity, and $\eta_N = 1$ will be used in the following. The plasma vorticity perturbation around the resonant surface induced by the RMP can be estimated by

$$U_1 \sim \phi_1/\delta^2, \tag{9}$$

where δ is the tearing layer width.

Depending on plasma viscosity and the normalized equilibrium plasma angular rotation frequency $\omega_N = \omega\tau_R$, there are two different regimes. When the viscous term is much larger than the inertia term in the plasma vorticity equation, i.e. the so-called visco-resistive regime [12], it is found from equation (8) that

$$S^2(ik_\parallel j_1 + b_{1r}j_{0/0}') + \mu_N\nabla_\perp^2 U_1 = 0\,. \tag{10}$$

In the outer region away from the resonant surface, the plasma viscosity is negligible, so that

$$ik_\parallel j_1 + b_{1r}j_{0/0}' = 0. \tag{11}$$

When approaching the resonant surface at r_s, $k_\parallel \approx k'_\parallel x$, and $j_1 \sim 1/x$, where $x = (r - r_s)$.

In the inner region around the resonant surface, the viscosity becomes important. Using (9), it is found from (10) and (7) that

$$iS^2 k'_\parallel \delta j_1 \sim \mu_N \phi_1 \delta^{-4}. \tag{12}$$

$$ik'_\parallel \delta \phi_1 \sim j_1, \tag{13}$$

where we have used δ for x and δ^{-2} for $\nabla_\perp^2$ as an estimation. The tearing layer width is found from (12)-(13) to be

$$\delta \sim \mu_N^{1/6} (S k'_\parallel)^{-1/3}. \tag{14}$$

It is also found from Ohm's law that

$$-i\omega_N \psi_1 \sim j_1. \tag{15}$$

In the framework of single fluid equations, $\Delta j_{0/0}$ is simply due to the nonlinearity contained in the $\boldsymbol{v}\cdot\nabla\psi$ term in Ohm's law, which is a static electric field approximately given by

$$\Delta j_{0/0} \sim ik_p \psi_1 \phi'_1 \tag{16}$$

near the resonant surface, where one also has

$$\phi'_1 \sim \phi_1/\delta. \tag{17}$$

Relations (12)-(17) lead to

$$\Delta j_{0/0} \sim k_p (k'_\parallel)^{-1/3} |\psi_1|^2 \omega_N S^{2/3} \mu_N^{-1/3}, \tag{18a}$$

or in the form

$$\Delta j_{0/0} \sim k_p (k'_\parallel)^{-1/3} |\psi_1|^2 \omega \tau_R^{2/3} S^{2/3} (a^2/\mu)^{1/3}, \tag{18b}$$

with ω in the unit of rad/s and μ in the unit of m^2/s. The amplitude of $\Delta j_{0/0}$ is proportional to $\omega \tau_R^{2/3} S^{2/3}$. For given values of ω and RMP amplitude, $\Delta j_{0/0}$ is larger for a smaller plasma resistivity ($\sim \tau_R^{4/3}$) and/or Alfven time. The change in the local current density gradient is approximately

$$\Delta j'_{0/0} \sim \Delta j_{0/0}/\delta \sim k_p |\psi_1|^2 \omega \tau_R^{1/2} S (a^2/\mu)^{1/2}, \tag{19}$$

which can be significant even for a small RMP amplitudes below the penetration threshold. Using the input parameters for the *low resistivity case*, detailed in the Appendix, $S = 2.6 \times 10^8$, $m = 4$, $r_s = 0.3m$, $\tau_R = 23s$, and $\mu = 0.2m^2/s$, and assuming $\omega = 10^4\, rad/s$ and $|\psi_1| = 10^{-7}$, one finds that $\Delta j'_{0/0} \sim 0.93 B_{0t}/a^2$, being larger than j'_0 which is usually of the order $B_p/a^2 \sim 0.1 B_{0t}/a^2$, where B_p is the poloidal magnetic field.

In the opposite limit, if the viscous term is much smaller than the inertia term in the plasma vorticity equation, one finds from equation (8) that

$$S^2 k_\parallel' j_1 \sim \omega_N \phi_1 \delta^{-3}\ , \tag{20}$$

Relations (13), (15)-(17) and (20) lead to

$$\delta \sim (\omega_N)^{1/4} (S k_\parallel')^{-1/2}, \tag{21}$$

$$\Delta j_{0/0} \sim k_p |\psi_1|^2 \omega_N^{1/2} S. \tag{22}$$

The change in the local current density gradient is approximately

$$\Delta j_{0/0}' \sim \Delta j_{0/0}/\delta \sim k_p |\psi_1|^2 (\omega \tau_R)^{1/4} S^{3/2} (k_\parallel')^{1/2}\ , \tag{23}$$

being proportional to $\tau_R^{1/4} S^{3/2}$.

Both (19) and (23) indicate that $\Delta j_{0/0}'$ is proportional to $|\psi_1|^2$ and is larger for a smaller plasma resistivity and/or Alfven time.

2.2 Numerical results

To take the full nonlinear effects into account for realistic RMP amplitude, numerical calculations based on equations (A1)-(A4) in the Appendix have been carried out to study the effect of $m/n = 4/2$ and $6/3$ RMPs on the local $\Delta j_{0/0}$ profile. The effect of RMPs of an m/n component is taken into account by the boundary condition

$$\psi_{m/n}|_{r=a} = \psi_{a,m/n} a B_t cos\ (m\theta + n\phi + \omega_{RMP} t), \tag{24}$$

where $\psi_{a,m/n}$ is the normalized amplitude of the m/n component helical flux at $r = a$, θ and ϕ are the poloidal and toroidal angles, and ω_{RMP} is the angular frequency of the applied RMP, taken to be zero if not specified. The numerical convergence has been checked with a radial grid size of $3 \times 10^{-4} a$ and 20 Fourier components.

The radial profile of the original equilibrium plasma current density is of the form $j_0 \sim [1 - (r/a)^2]^2$, leading to a monotonic q-profile with the $q = 2$ surface located at $r_s = 0.628a$. Without applying the RMP, the $4/2$ and the $6/3$ modes are linearly stable for this q-profile. Static RMPs of sufficiently small amplitude are applied such that they have not penetrated in for all the results presented in this subsection.

The input parameters are based on medium size tokamak experimental parameters: $T_e = 2keV$, $n_e = 3 \times 10^{19} m^{-3}$, $a = 0.5m$, $R = 1.7m$, and $B_t = 2T$. A parabolic profile for the original equilibrium electron density is assumed, and the equilibrium electron diamagnetic drift frequency is $\omega_{*e0} = 3.14 \times 10^5/\tau_R$ $(f_{*e0} = 2.17kHz)$ at the $q = 2$ surface for $m = 4$ and $\Omega = 2 \times 10^4$. The local bootstrap current density fraction at the $q = 2$ surface is $f_b = 0.35$. These parameters will be referred to as the *low resistivity case* and used as input for our calculations in the following, except when specified otherwise.

The normalized (to ω_{*e0}) bi-normal equilibrium electron fluid frequency at r_s is defined as

$$\omega_n = (1 - \omega_0), \tag{25}$$

where $\omega_0 = -\omega_{E0}/\omega_{*e0}$. A negative (positive) value of ω_n (ω_0) corresponds to a bi-normal electron fluid (**E**×**B** rotation) velocity in the ion drift direction. When the poloidal electric drift is negligible, a negative value of ω_n corresponds to an electric drift in the plasma current direction with a frequency being larger than the electron diamagnetic drift frequency (see Appendix B).

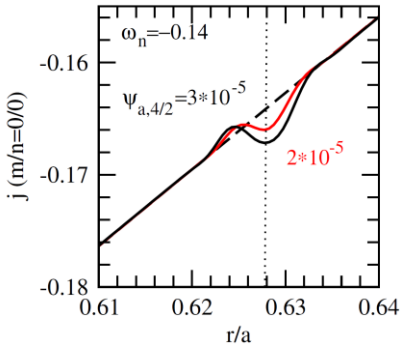

Figure 1 Radial profiles of the (normalized) $j_{0/0}$ in steady state for $\psi_{a,4/2} = 2 \times 10^{-5}$ (red curve) and 3×10^{-5} (black) with $\omega_n = -0.14$. The dashed curve is the original equilibrium plasma current density, being negative in our calculations. The location of the $q = 2$ surface is marked by the vertical dotted line.

In figure 1 the local radial profiles of $j_{0/0}$ in steady state are shown for $\psi_{a,4/2} = 2 \times 10^{-5}$ (red curve) and 3×10^{-5} (black) with $\omega_n = -0.14$. The dashed curve is the original equilibrium plasma current density before applying the $4/2$ RMP, taken to be negative in our calculations. It is seen that for a normalized $\psi_{a,4/2}$ in the order of 10^{-5}, the relative variation in the $j_{0/0}$ amplitude is small. However, the local $j_{0/0}$ gradient is significantly changed by the $4/2$ RMPs around the $q = 2$ surface, marked by the vertical dotted line, and this change increases for a larger RMP amplitude. More importantly, the local radial gradient of $j_{0/0}$ is reversed on the inner side of the $q = 2$ surface but is increased on the outer side for this ω_n value. This effect is similar to that caused by a localized electron cyclotron current drive (ECCD) at the $q = 2$ surface in the plasma current direction. For $\psi_{a,4/2} = 3 \times 10^{-5}$, the $4/2$ island width is $0.0084a$.

To investigate the role of plasma rotation, in the following we use $\omega_n = -0.7, -2.4$ and -3.6 (by varying the value of ω_{E0}) for a RMP amplitude $\psi_{a,4/2} = 10^{-4}$. Figure 2 (left) shows the corresponding radial profiles of $j_{0/0}$ in steady state. A negative value of ω_n (the electron fluid velocity in the ion diamagnetic drift direction) results in a larger (reversed) local current density gradient outside (inside) the $q = 2$ surface, which is known to be stabilizing for the tearing mode. Figure 2 (right) is the same as the left figure but for the electron fluid velocity in the electron drift

direction with $\omega_n = 1.6,\ 2.1,\ 3.8$ and 5.0. For $\omega_n = 1.6$, the local current density gradient inside the $q = 2$ surface is increased except in a very thin layer at the surface, being destabilizing for the tearing mode compared to the non-RMP case. For a sufficiently large value of ω_n, $\omega_n = 5$, however, the changes to the current density profile become stabilizing again.

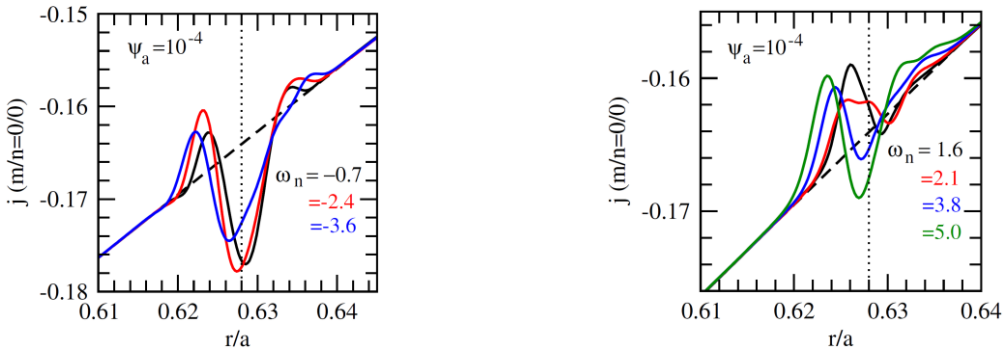

Figure 2 *With $\psi_{a,4/2} = 10^{-4}$ for the low resistivity case, radial profiles of (normalized) $j_{0/0}$ in steady state for (left) $\omega_n = -0.7,\ -2.4$ and -3.6; (right) $\omega_n = 1.6,\ 2.1,\ 3.8$ and 5.0.*

Two-fluid effects are found to be important for the change of the local $j_{0/0}$ profile in the *low resistivity case*. The electron diamagnetic drift frequency is proportional to the value of Ω in equation (A2) in the Appendix for a given equilibrium electron density profile. Artificially increasing Ω in the calculations results in a larger change in the local $j_{0/0}$ by RMPs. The reason is the stronger effective electric field resulting from the parallel electron pressure gradient in Ohm's law.

The effect of electron inertia on $j_{0/0}$ in the presence of RMPs is demonstrated in figure 3, showing radial profiles of $j_{0/0}$ in steady state for $\omega_n = -3.5$ and $\psi_{a,4/2} = 2 \times 10^{-4}$ with (black curve) and without (red) including the electron inertia. The electron inertia results in a larger change of the local $j_{0/0}$ at $q = 2$ surface in this case.

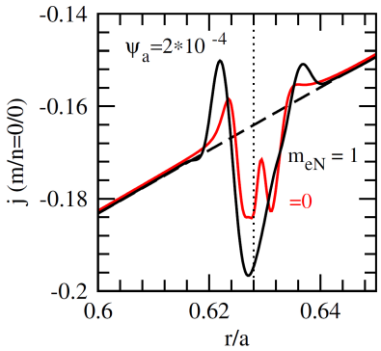

Figure 3 *Radial profiles of $j_{0/0}$ in steady state with (black curve) and without (red) including the electron inertia for $\omega_n = -3.5$ and $\psi_{a,4/2} = 2 \times 10^{-4}$.*

It is known that RMPs can affect the electron density profile, increasing (decreasing) the local

electron density gradient of the $0/0$ component for the electron fluid velocity in the ion (electron) drift direction [18], which causes a corresponding increase (decrease) in the local bootstrap current density, since the bootstrap current density is proportional to plasma density gradient. In figure 4, radial profiles of $j_{0/0}$ in steady state are shown for $\omega_n = -1.3$ and $\psi_{a,4/2} = 10^{-4}$ by taking the equilibrium bootstrap current density fraction $f_b = 0$ (black curve) and 0.35 (red). The dashed curve is the original equilibrium plasma current density, being the same for both cases. Including the bootstrap current density in the calculation, RMPs cause a larger change in the local $j_{0/0}$ at the $q = 2$ surface in this case due to the changed local bootstrap current density of the $0/0$ component [44].

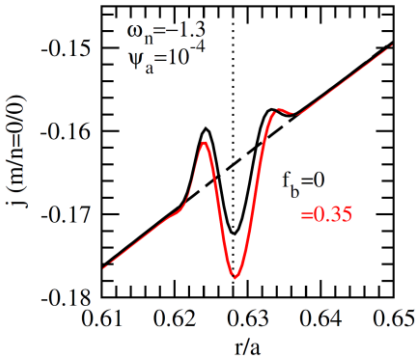

Figure 4 *Radial profiles of $j_{0/0}$ in steady state for $\omega_n = -1.3$ and $\psi_{a,4/2} = 10^{-4}$ with the equilibrium bootstrap current density fraction $f_b = 0$ (black curve) and 0.35 (red). The dashed curve is the original equilibrium plasma current density, being the same for both cases.*

Similar results are also found by applying $m/n = 6/3$ or $8/4$ RMPs below their penetration threshold. As an example, figure 5 shows the effect of a $6/3$ RMP with the amplitudes $\psi_{a,6/3} = 3 \times 10^{-5}$ (red curve) and 5×10^{-5} (black) for $\omega_n = -1.27$. The local radial profile of $j_{0/0}$ is changed in a similar way to the $4/2$ RMP case.

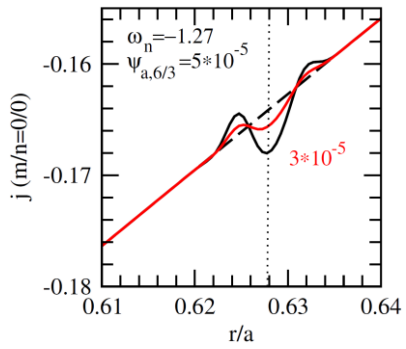

Figure 5 *For the case of an $m/n = 6/3$ RMP, radial profiles of $j_{0/0}$ in steady state for $\psi_{a,6/3} = 3 \times 10^{-5}$ (red curve) and 5×10^{-5} (black) with $\omega_n = -1.27$.*

Next we study a case with a higher resistivity, for which we chose the following set of

parameters as characteristic for a smaller size tokamak: $T_e = 300eV$, $n_e = 10^{19}m^{-3}$, $a = 0.25m$, $R = 1m$, and $B_t = 2T$. The local electron diamagnetic drift frequency is $\omega_{*e0} = 6.43 \times 10^3/\tau_R$ at the $q = 2$ surface. Furthermore, $f_b = m_e = 0$ is assumed. This case will be referred to as the *high resistivity case* in the following. Figure 6 shows an example for this *high resistivity case*, with $\psi_{a,4/2} = 3 \times 10^{-4}$ and $\omega_n = -11.5$ obtained from the two-fluid simulation (solid black curve). The red curve is obtained from single fluid equation by only solving equations (A2)-(A3) for the same values of $\psi_{a,4/2}$ and ω_n with $\Omega = 0$. Significant changes in the current density profile are found for both cases, however, only for sufficiently larger RMP amplitudes and plasma rotation velocities.

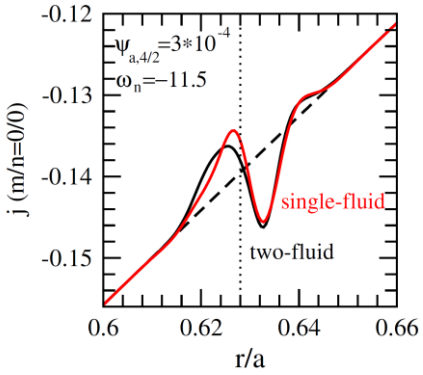

Figure 6 *Radial profiles of $j_{0/0}$ in steady state for the high resistivity case with $\psi_{a,4/2} = 3 \times 10^{-4}$ and $\omega_n = -11.5$. The solid black (red) curve is obtained from the four-field (single fluid) equations. The dashed curve is the equilibrium plasma current density.*

3. Effect of RMPs on $2/1$ island growth

In order to assess the role of the changed equilibrium current density by RMPs for MHD instabilities, driven or partly driven by the plasma current density gradient, in the following Section 3.1 the effects of static $m/n = 4/2$ and $6/3$ RMPs on the $2/1$ mode growth will be studied. Without applying RMPs, the $2/1$ tearing mode is unstable for the q-profile used here, and the magnetic island grows to a width of $0.2a$ in the nonlinear phase even when the bootstrap current perturbation is neglected. The effect of the $2/1$ RMPs on the $2/1$ NTM growth will be presented in Section 3.2 for comparison. The initial $2/1$ island width at $t = 0$ is smaller than $0.01a$ when applying static RMPs for all the results in Sections 3.1 and 3.2. The influences of a large initial $2/1$ island width and rotating RMPs are described in Section 3.3. Further including the electron temperature perturbations in calculations by solving the electron heat transport equation together with the four-field equations, the results are shown in Section 3.4.

3.1 Effect of static $m/n = 4/2$ and $6/3$ RMPs on $2/1$ island growth

In order to separate the underlying physics for a better understanding, in the following Section 3.1.1 linear results obtained from the single fluid equations are presented, to study the effect of the modified equilibrium current density by RMPs on the stability index Δ' and the linear growth rate of resistive tearing modes. Results obtained from four-field equations are given in Section 3.1.2, followed by the regimes for the $2/1$ mode stabilization by RMPs in Section 3.1.3.

3.1.1 Linear results from single fluid equations

It is well known that the value of Δ' determines the stability of resistive tearing mode. The Δ' values calculated from equation (11) are shown as a function of $-\omega_n$ in figure 7 (left), using the modified $j_{0/0}$ profile obtained from the four-field equations at different ω_n values in steady state with a $4/2$ RMP below the penetration threshold, $\psi_{a,4/2} = 10^{-4}$, as shown in figure 2. The dotted line marks the Δ' value for the original equilibrium current density unaffected by RMPs. The Δ' value becomes negative with the modified $j_{0/0}$ for the electron fluid velocity in the ion drift direction ($-\omega_n > 0$) or a sufficiently large $|\omega_n|$, but it is increased for $\omega_n \sim 2$ compared to the original one, as expected from the $j_{0/0}$ profiles shown in figure 2. For $\omega_n = 0$ or 1, the $4/2$ RMP has penetrated in.

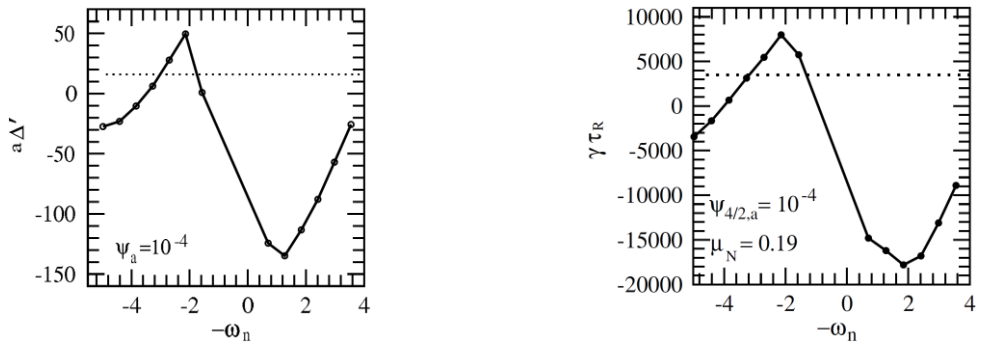

Figure 7 (left) The normalized Δ' value of the $2/1$ mode versus $-\omega_n$, with the input equilibrium current density obtained from the four-field equations for $\psi_{a,4/2} = 10^{-4}$. The dotted line marks the Δ' for the original equilibrium current density. (right) Corresponding to the left figure with the modified equilibrium current density as input, the normalized linear $2/1$ tearing mode growth rate versus $-\omega_n$, obtained from the single fluid equations for $S = 2.6 \times 10^8$ and $\mu_N = 0.19$. The dotted line marks the growth rate for the original equilibrium current density.

Corresponding to figure 7 (left) with the modified $j_{0/0}$ as input, the linear $2/1$ mode growth rate in the absence of RMPs, obtained from the single fluid equations for $S = 2.6 \times 10^8$ and $\mu_N = 0.19$, is shown by the solid curve in figure 7 (right). The dotted line marks the growth rate using the original equilibrium current density as input. The change of the linear growth rate at different ω_n

values with the modified $j_{0/0}$ is similar to that of the Δ'. The difference in the detailed profiles between the left and right figures is due to the the "constant-ψ" assumption used in Δ' calculations. This assumption is not well satisfied when there is a significant change of the local $j_{0/0}$ gradient around the resonant surface, as shown in figure 2. The linear growth rate is more accurate than the Δ' value in revealing the effect of the modified equilibrium current density on the mode stability.

3.1.2 Results from four-field equations

In this subsection the results are obtained by directly solving the four-field equations.

In the presence of small $4/2\ (6/3)$ RMPs below their penetration threshold for the *low resistivity case*, the linear $2/1$ mode growth rate is shown in figure 8 as a function of ω_n with $\psi_{a,4/2} = 2 \times 10^{-5}$ (black curve) and $\psi_{a,6/3} = 4 \times 10^{-5}$ (red). The dotted line marks the linear $2/1$ mode growth rate without applying RMPs, which changes little with ω_n. The growth rate is decreased by the $4/2\ or\ 6/3$ RMPs for the electron fluid velocity in ion drift direction $(-\omega_n > 0)$ or a sufficiently large value of $|\omega_n|$, but it is increased in the region $-\omega_n = [0,2]$, similar to the results obtained from single fluid equations shown in figure 7. When the value of $-\omega_n$ is slightly negative, the $4/2$ RMP has penetrated.

The linear growth rate shown in figures 7 and 8 is determined by the modified $j_{0/0}$ profile, as seen from figure 7(a), and the interaction between the 4/2 and 2/1 components, but it shows no stabilizing effect from plasma rotation shear due to the large S number (2.6×10^8) and small plasma viscosity used in calculations. The stabilizing effect from plasma rotation shear exists for a sufficiently low S value and/or large plasma viscosity [45,46].

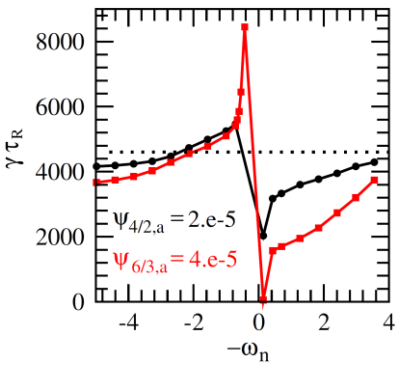

Figure 8 In the presence of $4/2\ (6/3)$ RMPs below their penetration threshold for the low resistivity case, the linear $2/1$ mode growth rate is shown as a function of ω_n with $\psi_{a,4/2} = 2 \times 10^{-5}$ (black curve) and $\psi_{a,6/3} = 4 \times 10^{-5}$ (red). The dotted line marks the linear $2/1$ mode growth rate without applying RMPs. The growth rate is decreased by the $4/2$ or $6/3$ RMPs for $-\omega_n > 0$ or a sufficiently large $|\omega_n|$.

For the *low resistivity case* with $\omega_n = 0$, the time evolution of the normalized $m/n = 2/1$ magnetic island width, calculated from $W = 4[\psi_{2/1}/(B_p q'/q)]^{1/2}$ at the $q = 2$ surface, is shown in Figure 9 for $\psi_{a,4/2} = 0,\ 1.5 \times 10^{-5}$ and 3×10^{-5}. The $2/1$ island growth is speeded up already by small $4/2$ RMPs. Similar results are also found for $\omega_n = 1$, as expected from the results shown in figure 8.

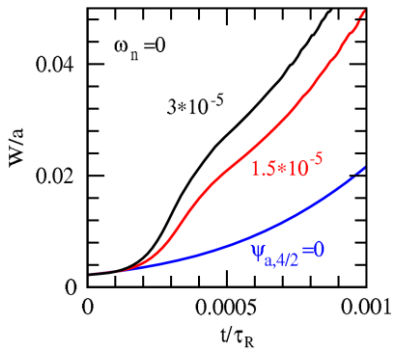

Figure 9 *For the low resistivity case with $\omega_n = 0$, time evolution of the $2/1$ island width for $\psi_{a,4/2} = 0,\ 1.5 \times 10^{-5}$ and 3×10^{-5}. A small $4/2$ RMP speeds up the $2/1$ island growth.*

For the electron fluid velocity in the ion drift direction with $\omega_n = -0.14$, the time evolution of the normalized $2/1$ island width is shown in Figure 10 for $\psi_{a,4/2} = 0, 2 \times 10^{-5}$ and 3×10^{-5}. A small $4/2$ RMP, $\psi_{a,4/2} = 3 \times 10^{-5}$, stabilizes the $2/1$ island growth, partly due to the change of the local $j_{0/0}$ profile around $q = 2$ surface as shown in figure 1. Using a smaller RMP, $\psi_{a,4/2} = 2 \times 10^{-5}$, the $2/1$ island growth is slowed down in the early phase, but is not stabilized.

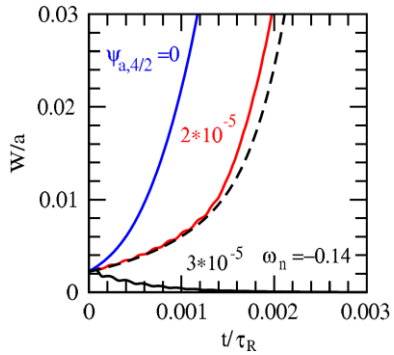

Figure 10 *For the low resistivity case with $\omega_n = -0.14$, time evolution of the $2/1$ island width for $\psi_{a,4/2} = 0$ (blue curve), 2×10^{-5} (red) and 3×10^{-5} (solid black). A small $4/2$ RMP, $\psi_{a,4/2} = 3 \times 10^{-5}$, stabilizes the $2/1$ island growth. When using the $j_{0/0}$ in steady state obtained with $\psi_{a,4/2} = 3 \times 10^{-5}$ as the input equilibrium current density, the $2/1$ island growth without applying RMPs is shown by the dashed curve.*

To identify the effect of the current density profile modifications by RMPs, we have used the

$j_{0/0}$ profile obtained in steady state with $\psi_{a,4/2} = 3 \times 10^{-5}$ as the input equilibrium current density to calculate the $2/1$ mode growth without applying RMPs. The corresponding result is shown by the dashed curve in figure 10. In this case the $2/1$ mode is still unstable, but grows more slowly in the earlier phase compared to the case with the original equilibrium current density (blue curve). This indicates that the change of $j_{0/0}$ by the RMP is not the sole mechanism for stabilizing the $2/1$ mode.

Applying a static RMP to a rotating plasma, the total equilibrium magnetic field becomes a weakly three-dimensional one, including a helical shielding plasma current density, which can also affect the MHD instability in addition to the change of $j_{0/0}$. For example, in the presence of a small $4/2$ RMP, the linear growth of the $2/1$ plasma vorticity is given by

$$\gamma U_{2/1} = iS^2[k_\parallel j_{2/1} + (2/r)\psi_{2/1}(j'_{0/0} + 0.5j'_{4/2}) + (2/r)\psi_{4/2}j'_{2/1}] + \mu_N \nabla_\perp^2 U_{2/1}, \quad (26)$$

where the coupling between the $4/2$ and $2/1$ component plasma velocity and vorticity perturbations and higher order terms being proportional to $\psi'_{2/1}j_{4/2}$ and $\psi'_{4/2}j_{2/1}$ are neglected. As the terms involving $\psi_{2/1}j'_{4/2}$ and $\psi_{4/2}j'_{2/1}$ in equation (26) are of the same order of magnitude, the effect of the $4/2$ RMP on the $2/1$ mode stability can be assessed by the ratio of $0.5j'_{4/2}/j'_{0/0}$. At the resonant surface [18]

$$j_{4/2} = i\omega_{e\perp N}\psi_{4/2}, \quad (27)$$

which has a radial width being about the tearing layer width, so that

$$j'_{4/2} \sim i\omega_{e\perp N}\psi_{4/2}/\delta\ . \quad (28)$$

As

$$\psi_{4/2} = W_{4/2}^2 B_p q'/(16q), \quad (29)$$

where $W_{4/2}$ is the 4/2 island width, and $j'_{0/0} \sim B_p/a^2$, one finds

$$0.5j'_{4/2}/j'_{0/0} \sim 0.5i\omega_{e\perp N}(W_{4/2}^2/a\delta)aq'/(16q). \quad (30)$$

Assuming $\delta = W_{4/2} = 0.005a$, $aq'/q = 1$, $\omega_{e\perp N} = 10^4$, one finds from (30) that $0.5j'_{4/2}/j'_{0/0} \sim 1.6$, indicating that a small $4/2$ RMP can affect the $2/1$ mode stability even if the change of $j_{0/0}$ discussed in Section 2 is neglected.

The effect described in (26) to (30) is proportional to the RMP amplitude. The change of $j_{0/0}$ is proportional to the square of the RMP amplitude, which is expected to be more important in determining the $2/1$ mode stability for larger RMPs. Similar to the case shown by the dashed curve in figure 10, calculations have also been carried out for a larger $4/2$ RMP at a larger value of $|\omega_n|$. In such cases the change of $j_{0/0}$ alone is found to be sufficient for stabilizing the $2/1$ mode.

By applying the $m/n = 4/2$ (black curve) and $6/3$ (red) RMPs separately below their

penetration threshold with $\omega_n = -1.27$, it is seen from figure 11 that the linear growth rate of the $2/1$ mode almost linearly decreases with the square of the normalized RMP amplitude, $\psi^2_{a,m/n}$, for a sufficiently large RMP, as expected. The growth rate decreases faster with increasing the RMP amplitude for the $4/2$ RMP. The $4/2$ island width, being proportional to the square root of the local $4/2$ magnetic perturbation amplitude, is larger than the $6/3$ island width at the same value of $\psi^2_{a,m/n}$, but it is smaller than $0.01a$ for all cases shown in figure 11.

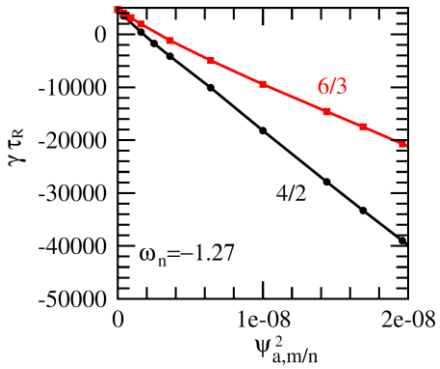

Figure 11 *By applying $m/n = 4/2$ (black curve) and $6/3$ (red) RMPs separately with $\omega_n = -1.27$, the linear $2/1$ mode growth rate is shown as a function of the square of the normalized RMP amplitude. The growth rate almost linearly decreases with the square of the RMP amplitude for a sufficiently large RMP.*

3.1.3 Regimes for $2/1$ mode stabilization

Extensive nonlinear simulations based on four-field equations have been carried out by scanning over the values of the plasma rotation velocity and the $4/2$ RMP amplitude, while keeping the other input parameters unchanged. The stability diagram in the $(\omega_n - \psi_{a,4/2})$ plane is shown in Figure 12 (left) for the *low resistivity case*. The black circles (red squares) are the cases in which the $2/1$ island growth is (not) stabilized by the $4/2$ RMP. A large stabilization region exists for the electron fluid velocity in the ion drift direction ($-\omega_n > 0$). When the value of $|\omega_n|$ is sufficiently large, a stabilization region also exists for $-\omega_n < 0$ but it is smaller than that for $-\omega_n > 0$. The asymmetry on the two sides of $\omega_n = 0$ can be understood from the dependence of the linear growth rate on the value of ω_n as shown in figures 7 and 8. The upper boundary of the stabilization region is determined by the $4/2$ RMP penetration threshold in the presence of the $2/1$ perturbation. Once the RMP is sufficiently large, the local bi-normal electron fluid velocity is significantly reduced due to the change of both the plasma rotation velocity and electron density gradient, similar to that described in Ref. [18,20,21]. A large value of $|\omega_n|$ leads to a larger threshold for the RMP penetration and therefore a wider stabilization region. The lower boundary of the stabilization region is determined by the minimum $4/2$ RMP to have a large enough stabilizing effect, as shown in figure

10. For the *low resistivity* case, no $2/1$ mode stabilization by the $4/2$ RMP has been found from single fluid equations for the value of $|\omega_n|$ up to 5, being quite different from the two-fluid simulation results.

Figure 12 (right) shows results for the *high resistivity case*. The black circles (red squares) are again the cases in which the $2/1$ island growth is (not) stabilized by the $4/2$ RMP. In this case the stabilization region exists only for $|\omega_n| > 5$, and the stabilization region is nearly symmetric on the two sides of $\omega_n = 0$ for $|\omega_n| \sim 9$ or larger. The blue diamonds (green triangles) are single fluid results for which the $2/1$ island growth is (not) suppressed by the $4/2$ RMP. The stabilization window obtained from the four-field equations is different from that of the single fluid equations, indicating the role of two-fluid physics even for the *high resistivity* case.

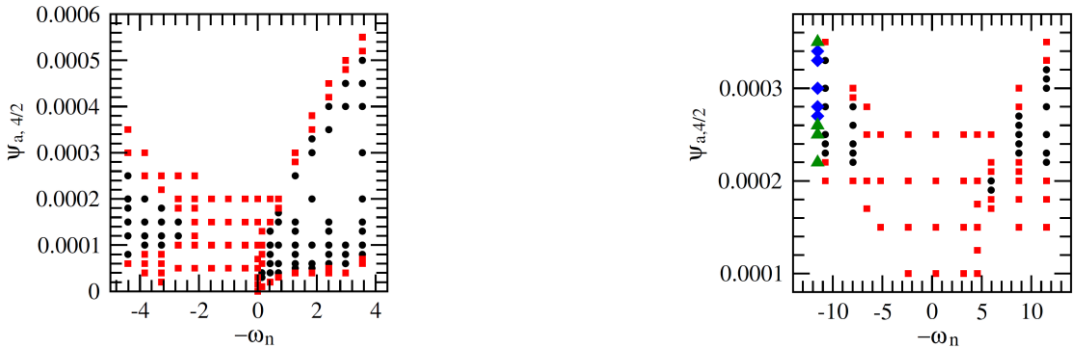

Figure 12 (left) Stability diagram in the $(\omega_n - \psi_{a,4/2})$ plane obtained from the four-field equations for the low resistivity case. The black circles (red squares) mark the cases in which the $2/1$ island growth is (not) stabilized by the $4/2$ RMP. The stabilization region is larger for the plasma rotation in the ion drift direction $(-\omega_n > 0)$. (right) Same as the left figure but for the high resistivity case. The stabilization region exists only for $|\omega_n| > 5$. The blue diamonds (green triangles) are single fluid results for which the $2/1$ island growth is (not) suppressed by the $4/2$ RMP.

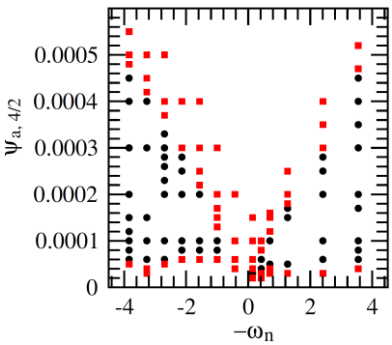

Figure 13 Same as figure 12 (left) for the low resistivity case but with $f_b = 0$. The black circles (red squares) are the cases in which the $2/1$ island growth is (not) stabilized by the $4/2$ RMP.

When the bootstrap current density fraction f_b is taken to be zero in the calculations for the

low resistivity case, while keeping the other input parameters the same as those for figure 12 (left), the stability diagram in the $(\omega_n - \psi_{a,4/2})$ plane is shown in Figure 13. The black circles (red squares) are again for the cases in which the $2/1$ island growth is (not) stabilized by the $4/2$ RMP. Without including bootstrap current density perturbations, the stabilization region is smaller for $-\omega_n > 0$ but is much larger for $-\omega_n < 0$, showing the role of the bootstrap current density perturbation in increasing the asymmetry [18,44].

By applying $6/3$ RMPs, the stability diagram in the $(\omega_n - \psi_{a,6/3})$ plane obtained from four-field equations is shown in figure 14 for the *low resistivity case*. The black circles (red squares) mean that the $2/1$ island growth is (not) stabilized by $6/3$ RMPs. The stabilization region by applying $6/3$ RMPs is similar to that by $4/2$ RMPs for $-\omega_n > 0$, but the required $6/3$ RMP amplitude is somewhat larger. The $6/3$ RMPs leads to a larger stabilization window for $-\omega_n < 0$ compared to the $4/2$ RMP case, since the intrinsic frequency of the $6/3$ mode is higher than that of the $4/2$ mode for the same value of ω_n. Both the diamagnetic drift and plasma rotation frequencies are proportional to the mode numbers.

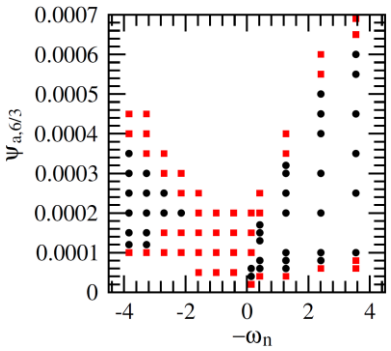

Figure 14 Same as figure 12 (left) for the low resistivity case but by applying the $6/3$ RMPs. The black circles (red squares) are the cases in which the $2/1$ island growth is (not) stabilized by the $6/3$ RMP.

3.2 Effect of $2/1$ RMPs on $2/1$ island growth

As already shown in references [4,9,33], a $2/1$ RMP can also suppress the $2/1$ mode growth. By applying $2/1$ RMPs, the stability diagram in the $(\omega_n - \psi_{a,2/1})$ plane obtained from four-field equation is shown in figure 15 (left) for the *low resistivity* case. The black circles (red squares) are the cases that the island growth is (not) stabilized by the $2/1$ RMP. A larger RMP is required for NTM's onset or RMP penetration for a larger value $|\omega_n|$, being in line with the experimental observation that NTMs are more stable for a larger plasma rotation velocity [47,48]. The stabilization regions are also asymmetric on the two sides of $\omega_n = 0$, as observed in the RMP penetration experiments [8], but they are smaller compared to the $4/2$ or $6/3$ RMP cases for $-\omega_n < 0$. This

indicates again that static RMPs of higher harmonics have a larger window in the region $-\omega_n < 0$ to stabilize the $2/1$ mode.

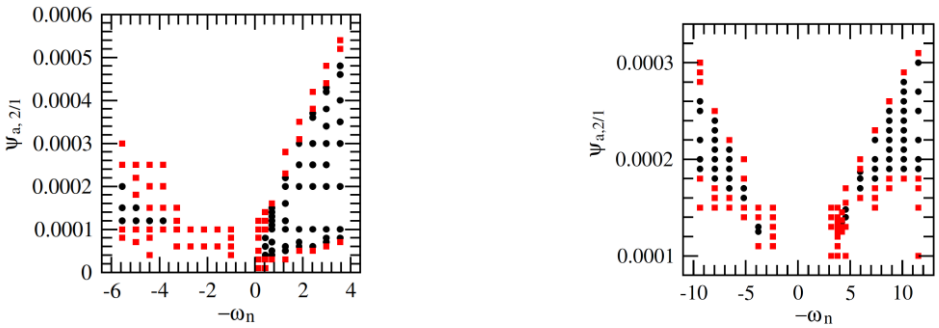

Figure 15 (left) Stability diagram in the $(\omega_n - \psi_{a,2/1})$ plane for the low resistivity case obtained from four-field equation. The black circles (red squares) are the cases in which the island growth is (not) stabilized by the $2/1$ RMP. (right) same as the left figure but for the high resistivity case.

For the *low resistivity* case, no $2/1$ mode stabilization by the $2/1$ RMP has been found from single fluid equations for the value of $|\omega_n|$ up to 5.

Figure 15 (right) is same as the left figure but for the *high resistivity* case. In this case, the stabilization region only exists for sufficiently large ω_n values ($\omega_n > 4$), and it is nearly symmetrical on the two sides of $\omega_n = 0$. Comparing to the effect of the $4/2$ RMPs for the *high resistivity* case shown in figure 12 (right), the stabilization region by applying the $2/1$ RMP is larger in the region $|\omega_n| < 10$. This could be due to the $2/1$ ion polarization current and the non-uniform $2/1$ island rotation caused by the $2/1$ RMP [4,9,12,33].

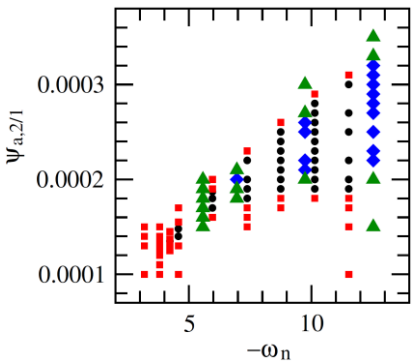

FIG. 16. Stability diagram in the $(\omega_n - \psi_{a,2/1})$ plane for the high resistivity case. The blue diamonds (green triangles) are the cases in which the $2/1$ island growth is (not) suppressed by $2/1$ RMPs for the single fluid case. The black circles and red squares are obtained from four-field equation, being the same as those in figure 15 (right) for $-\omega_n > 0$.

To compare the results obtained from the single fluid and four-field equations, the stability diagram in the $(\omega_n - \psi_{a,2/1})$ plane is shown in figure 16 for the *high resistivity* case. The blue

diamonds (green triangles) are the cases in which the $2/1$ island growth is (not) suppressed by the $2/1$ RMP for the single fluid case. The black circles and red squares are the same as those shown in figure 15 (right), obtained from four-field equations for $-\omega_n > 0$. The stabilization region obtained from four-field equations is larger than that from the single fluid equations for $-\omega_n < 10$, indicating again the role of two-fluid physics for the *high resistivity* case.

3.3 Effect of initial 2/1 island width and rotating RMP

The results shown in Sections 3.1 and 3.2 were obtained with a small initial $2/1$ island width at $t = 0$ when applying static RMPs. If the initial $2/1$ island width is too large, the island growth cannot be stabilized by RMPs. As an example, the time evolution of the normalized $2/1$ island width is shown in figure 17 by applying the $4/2$ RMP for different initial $2/1$ island widths, with $\omega_n = -3.5$ and $\psi_{a,4/2} = 3 \times 10^{-4}$ for the *low resistivity case*. The $2/1$ island grows for a larger initial width (red curve) but is stabilized for a slightly smaller one (black), showing a threshold in the initial $2/1$ island width. For a sufficiently large island the local electron density profile flattens, and the two-fluid effects such as the diamagnetic drift vanish.

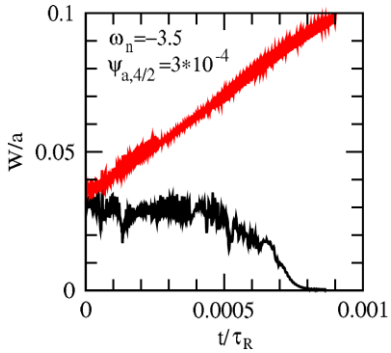

Figure 17 By applying $4/2$ RMP with $\omega_n = -3.5$ and $\psi_{a,4/2} = 3 \times 10^{-4}$ for the low resistivity case, the time evolution of normalized $2/1$ island width for different initial $2/1$ island width. The $2/1$ island grows for a larger initial width (red curve) but is stabilized for a smaller one (black).

As shown in Sections 3.1 and 3.2, static RMPs can suppress the $2/1$ island growth only for a negative value of ω_n or a sufficiently large $|\omega_n|$. Rotating RMPs should be able to stabilize the island in any case, since the result only depends on the relative rotation between the electron fluid and RMPs. An example is shown in figure 18 for the time evolution of the $2/1$ island width with $\omega_n = 0$ and $\psi_{a,4/2} = 10^{-4}$. The island grows for a low $4/2$ RMP angular frequency, $\omega_{RMP}/\omega_{*e0} = 0.16$, but is suppressed for $\omega_{RMP}/\omega_{*e0} = 0.32$. The RMP rotates in the electron diamagnetic drift direction, being more effective for the island suppression than it would be in the ion drift direction.

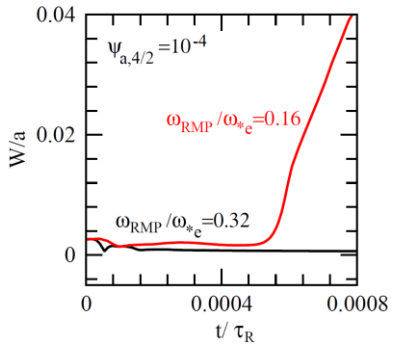

Figure 18 By applying rotating $4/2$ *RMPs for the low resistivity case with* $\omega_n = 0$ *and* $\psi_{a,4/2} = 10^{-4}$*, the time evolution of normalized* $2/1$ *island width for* $\omega_{RMP}/\omega_{*e0} = 0.16$ *(red curve) and* 0.32 *(black). The RMP rotates in the electron diamagnetic drift direction.*

3.4 Effect of electron temperature perturbations

The electron temperature perturbations have been neglected for the results in Sections 3.1-3.3. When further including them by solving the electron heat transport equation, equation (A9) in the Appendix, together with the four-field equations, (A1)-(A4), the results are shown in figure 19. The black circles (red squares) are the cases in which the $2/1$ island growth is (not) stabilized by the $4/2$ RMP. Same input parameters as those of figure 12 (left) for the *low resistivity case* have been used. In addition, the ratio between the parallel and perpendicular heat conductivity, $\chi_\parallel/\chi_\perp = 10^9$, $\chi_\perp = \mu$, and a parabolic profile for the equilibrium electron temperature are taken. The equilibrium electron diamagnetic drift frequency $\omega_{*e0} = 9.74 \times 10^5/\tau_R$ ($f_{*e0} = 4.3kHz$) at the $q = 2$ surface for $m = 4$, being about two times larger than that for figure 12 (left) due to the additional contribution from the electron temperature gradient. The results are also asymmetry on the two sides of $\omega_n = 0$. A large stabilization region exists for $-\omega_n > 0$ but at a smaller value of $|\omega_n|$ than that shown in figure 12 (left). The range of the electric drift velocity in figure 19 is about the same as that in figure 12 (left). A larger electron diamagnetic drift frequency for figure 19 leads to a smaller value of $|\omega_n|$ for the same electric drift velocity. The upper boundary of the stabilization region depends on the electric drift velocity.

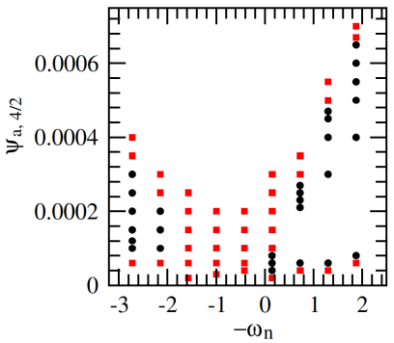

Figure 19 Stability diagram in the $(\omega_n - \psi_{a,4/2})$ *plane for the low resistivity case, obtained from the four-field equations together with the electron heat transport equation (A9). The black circles (red squares) mark the cases in which the* $2/1$ *island growth is (not) stabilized by the* $4/2$ *RMP.*

4. Discussion and summary

It is well known that the application of RMPs to rotating plasmas causes helical shielding currents at resonant surfaces as long as the fields don't penetrate, which is basically a linear effect. It is shown in this paper that due to nonlinear effects, the local $m/n = 0/0$ component plasma current density gradient can be changed by the helical shielding currents coupled to magnetic and plasma velocity perturbations, as seen from equation (1). The change of the local electron density gradient and bootstrap current density is also caused by the coupling of helical shielding currents and magnetic perturbations [18,44]. The current density profile modification is significant for RMPs of the order $\psi_a = 10^{-5} - 10^{-4}$ below their penetration threshold, being larger for a higher electron temperature and depending on the plasma rotation velocity. As the intrinsic error field in tokamaks is usually in the same order of magnitude, while the applied RMPs are even larger, they could change the local plasma current density profile around the resonant surface according to our results. The required error field or RMP amplitude to affect the local current density profile is expected to be even smaller for a fusion reactor with a low plasma resistivity.

Our results also indicate that moderate $4/2$ or $6/3$ RMPs below their penetration threshold affect a small $2/1$ island growth mainly due to the change of the local current density gradient around the resonant surface, which can be either stabilizing or destabilizing, depending on the plasma rotation velocity. Static RMPs of moderate amplitude are found to stabilize the $2/1$ island growth if the local bi-normal electron fluid velocity at $q = 2$ surface is in the ion drift direction or sufficiently large. Rotating RMPs of a sufficiently high frequency in the electron drift direction are more effective to stabilize the $2/1$ island growth independent of the electron fluid velocity.

In addition to the change of the local $m/n = 0/0$ component of the plasma current density gradient around the $q = 2$ surface, a moderate $4/2$ RMP below its penetration threshold also has a direct effect on the $2/1$ mode stability by introducing a new equilibrium. This weakly three-dimensional equilibrium, including a $4/2$ component magnetic field and the associated helical shielding current, makes the $2/1$ mode more stable, if the local electron fluid rotates in the ion drift direction.

As already shown in existing publications [4,9,12], a $2/1$ RMP can also suppress the $2/1$ mode growth. The conventional explanation of the stabilization is based on single-fluid simulation

results [4,9,12]: RMPs can cause a non-uniform mode rotation due to its applied electromagnetic torque. The island stays for a longer time in the half period when the RMP is stabilizing than in another half period when the RMP is destabilizing, resulting in a net stabilizing effect by RMPs [4,9,12]. In addition, the $2/1$ component of ion polarization current induced by RMPs is also involved [33]. As the stability diagrams obtained by applying the $2/1, 4/2$ *or* $6/3$ RMPs shown in Section 3.2 are similar for the *low resistivity case*, the change of the local flux-surface-averaged plasma current density gradient around $q = 2$ surface becomes increasingly important for stabilizing the $2/1$ mode with decreasing resistivity.

It has been observed in existing tokamak discharges that NTMs can significantly degrade tokamak plasma confinement. Among them, the $2/1$ NTM is the most dangerous one, which can grow to a large amplitude and cause major disruption, a critical issue to be solved for a fusion reactor. NTMs can be stabilized by ECCD if a sufficiently large driven current is accurately located at the resonant surface [49-56]. Recent theoretical studies, however, showed that the deposition width of the electron cyclotron wave will be $2 - 4$ times larger in ITER when taking into account plasma density perturbations [57], corresponding to a lower driven current density at the resonant surface and therefore a larger wave power required for NTM stabilization. Our results indicate that static or rotating RMPs of moderate amplitude, depending on the plasma rotation direction, provide a possible method to stabilize the small island, similar to preempting NTM by ECCD. The $4/2$ or $6/3$ RMPs will not generate locked $2/1$ mode even if their amplitude is large. For ITER plasmas with 17 MW neutral beam injection together with the intrinsic torque, the plasma rotation is predicted to be in the ion drift (co-current) direction with a rotation frequency being about one order of magnitude larger than the electron diamagnetic frequency [58]. Although the prediction involves uncertainty, moderate static $4/2$ or $6/3$ RMPs could have a strong stabilizing effect for small $2/1$ islands, as long as the electron fluid velocity is in the ion drift direction. However, once the NTM amplitude is sufficiently large, ECCD would still be required for NTM stabilization.

A significant change of the local flux-surface-averaged current density profile induced by RMPs might also be important for other MHD instabilities driven or partially driven by the plasma current density gradient.

In summary, it is found in this paper that

(a) The local flux-surface-averaged plasma current density gradient around the q=2 surface can be significantly changed by moderate $m/n = 4/2$ or $6/3$ RMPs below their penetration threshold, and the required RMP amplitude for this change becomes smaller for a higher electron temperature. The modified local current density profile depends on the bi-normal electron fluid velocity;

(b) The growth of small $m/n = 2/1$ islands, driven by an unfavorable plasma current density profile and bootstrap current perturbation, is found to be stabilized by static $m/n = 4/2$ or $6/3$ RMPs of moderate amplitude if the electron fluid velocity is in the ion drift (co-current) direction or sufficiently large in the electron drift direction;

(c) A weakly three-dimensional equilibrium, containing a moderate $m/n = 4/2$ or $6/3$ RMP together with the associated shielding current and the modified flux-surface-averaged plasma current density gradient, is more stable against the $2/1$ mode, if the local electron fluid rotates in the ion drift direction with respect to applied RMPs.

References

[1] Karger F. *et al* 1975 Plasma physics and controlled nuclear fusion research 1974 *Proc. 5th Int. Conf. (Tokyo, 1974)* vol 1 (Vienna: IAEA) p 207 (www-naweb.iaea.org/napc/physics/FEC/STIPUB381 VOL1.pdf)

[2] Zhao Q.C. *et al* 1985 Plasma physics and controlled nuclear fusion research 1984 *Proc. 10th Int. Conf. (London, 1984)* vol 1 (Vienna: IAEA) p 345 (www-naweb.iaea.org/napc/physics/FEC/STIPUB670 VOL1.pdf)

[3] Ellis J.J., Howling A.A., Morris A.W. and Robinson D.C. 1985 Plasma physics and controlled nuclear fusion research 1984 *Proc. 10th Int. Conf. (London, 1984)* vol 1 (Vienna:IAEA) p 363 (www-naweb.iaea.org/napc/physics/FEC/STIPUB670 VOL1.pdf)

[4] Hender T.C. *et al* 1992 *Nucl. Fusion* **32**, 2091

[5] Buttery R.J. *et al* 2000 *Nucl. Fusion* **40**, 807

[6] La Haye R.J., Fitzpatrick R., Hender T.C. *et al* 1992 *Phys. Fluids B* **4**, 2098

[7] Wofle S.W., Hutchinson I.H., Granetz R.S. *et al* 2005 *Phys. Plasmas* **12**, 056110

[8] Koslowski H.R., Liang Y., Krämer-Flecken A. *et al* 2006 *Nucl. Fusion* **46**, L1

[9] Hu Q., Yu Q., Rao B., Ding Y. H. *et al* 2012 *Nucl. Fusion* **52**, 083011

[10] Nave M.F.F. and Wesson J.A. 1990 *Nucl. Fusion* **30**, 2575

[11] Zohm H., Kallenbach A., Bruhns H. *et al* 1990 *Europhys. Lett*. **11**, 745

[12] Fitzpatrick R. 1993 *Nucl. Fusion* **33**, 1049

[13] Waelbroeck F. L. 2003 *Phys. Plasmas* **10**, 4040

[14] Yu Q., Günter S., Kikuchi Y. and Finken K.H. 2008 *Nucl. Fusion* **48**, 024007

[15] Yu Q. and Günter S 2008 *Nucl. Fusion* **48**, 065004

[16] Finken K.H., Abdullaev S.S., De Bock M.F.M. *et al* 2005 *Phys. Rev. Lett*, **94**, 015003

[17] Finken K.H., Abdullaev S.S., Jakubowski M.W. *et al* 2007 *Phys. Rev. Lett*, **98**, 065001

[18] Yu Q. and Günter S. 2009 *Nucl. Fusion* **49** 062001

[19] Hu Q., Yu Q., Wang N. *et al* 2014 *Nucl. Fusion* **54** 122006

[20] Yu Q., Günter S. and Finken K.H. 2009 *Phys. Plasmas* **16**, 042301

[21] Yu Q. and Günter S. 2011 *Nucl. Fusion* **51** 073030

[22] Evans T.E., Moyer R.A., Thomas P.R. *et al* 2004 *Phys. Rev. Lett*, **92**, 235003

[23] Liang Y. *et al* 2007 *Phys. Rev. Lett* **98** 265004

[24] Suttrop W. *et al* 2011 *Phys. Rev. Lett* **106** 225004

[25] Shoji T., Tamai H., Miura Y., Mori M. and Ogawa H. 1992 *J. Nucl. Mater.* **196** 296–300

[26] Kirk A. *et al*, MAST and ASDEX Upgrade Teams 2015 *Nucl. Fusion* **55** 043011

[27] Jeon Y. M. *et al* 2012 *Phys. Rev. Lett.* **109** 035004

[28] Suttrop W. *et al* 2017 *Plasma Phys. Control. Fusion* **59** 014049
[29] Nazikian R. *et al* 2015 *Phys. Rev. Lett* **114** 105002
[30] Hu Q. *et al*, 2020 *Phys. Rev. Lett.* **125**, 045001
[31] Hu Q. *et al*, 2019 *Phys. Plasmas* **26** 120702
[32] Hu Q. *et al*, 2020 *Nucl. Fusion* **60** 076001
[33] Yu Q., Günter S. and Lackner K. 2018 Nucl. Fusion **58** 054003.
[34] Smolyakov A.I. 1993 *Plasma Phys. Control. Fusion* **35** 657
[35] Wilson H.R., Connor J.W., Hastie R.J. and Hegna C.C. 1996 *Phys. Plasmas* **3** 248
[36] Connor J.W., Waelbroeck F.L. and Wilson H.R. 2001 *Phys. Plasmas* **8** 2835
[37] Sauter O. *et al* 1997 *Phys. Plasmas* **4** 1654
[38] Waelbroeck F.L., Connor J.W. and Wilson H.R. 2001 *Phys. Rev. Lett.* **87** 215003
[39] Fitzpatrick R., Waelbroeck F.L. and Militello F. 2006 *Phys. Plasmas* **13** 122507
[40] Waelbroeck F.L. and Fitzpatrick R. 1997 *Phys. Rev. Lett.* **78** 1703
[41] Yu Q. 2010 *Nucl. Fusion* **50** 025014
[42] Hazeltine R. D. *et al* 1985 *Phys Fluids* **28** 2466
[43] Ara, G. 1978 Ann. Phys. (NY) **112**, 443
[44] Yu Q., 2020 *Nucl. Fusion* **60** 084001
[45] Hu Q., Yu Q. and Hu X.W., 2014 Phys. Plasmas **21**, 122507
[46] Coelho R. and Lazzaro E., 2007 Phys. Plasmas **14**, 012101
[47] La Haye R.J., Petty C.C., Politzer P.A., and the DIII-D Team, 2011 Nucl. Fusion **51**, 053013
[48] La Haye R.J., Brennan D. P., Buttery R. J., and Gerhardt S. P., 2010 Phys. Plasmas **17**, 056110.
[49] Zohm H., Gantenbein G., Giruzzi G. *et al*. 1999 *Nucl. Fusion* **39** 577
[50] Gantenbein G., Zohm H., Giruzzi G. *et al.* 2000 *Phys. Rev. Lett*. **85** 1242
[51] Günter S., Giruzzi G., Gude A. *et al.* 1999 *Plasma Phys. Controlled Fusion* **41**, b231
[52] La Haye R.J., Günter S., Humphreys D. A. *et al*. 2002 *Phys. Plasmas* **9** 2051
[53] Isayama A., Kamada Y., Ide S. *et al*. 2000 *Plasma Phys. Controlled Fusion* **42**, L37
[54] Maraschek M., Gantenbein G., Yu Q. *et al* 2007 *Phys. Rev. Lett*. **98**, 025005
[55] Yu Q., Zhang X.D. and Günter S., 2004 *Phys. Plasmas* **11**, 1960
[56] Wang X.J., Yu Q., Zhang X.D. 2018 *Plasma Phys. Controlled Fusion* **60** 045004
[57] Poli E. *et al*. 2015 *Nucl. Fusion* **55** 013023
[58] Chrystal C. *et al* 2017 Phys. Plasmas **24**, 056113 (2017)

Appendix A Equations and input parameters

Using the large aspect ratio approximation, the magnetic field is defined as $\boldsymbol{B} = B_t\boldsymbol{e}_t - \left(k_t/k_p\right)B_t\boldsymbol{e}_p + \nabla\psi \times \boldsymbol{e}_t$, where B_t is the equilibrium toroidal field, ψ is the helical flux, $k_p = m/r$ and $k_t = n/R$ are the wave vectors in $\boldsymbol{e}_p$ (poloidal) and $\boldsymbol{e}_t$ (toroidal) direction, and r and R are the minor and the major radius. The ion velocity $\boldsymbol{v} = \boldsymbol{v}_\parallel + \boldsymbol{v}_E$, including both the parallel and perpendicular component, $\boldsymbol{v}_E = \nabla\phi \times \boldsymbol{e}_t$, and ϕ is the velocity stream function.

The four-field equations, the continuity equation, the generalized Ohm's law, the plasma vorticity equation, and the equation of motion in the parallel (to magnetic field) direction, are utilized [42]. The toroidal mode coupling is neglected. Normalizing the length to the plasma minor radius a, the time t to the resistive time $\tau_R = a^2\mu_0/\eta$ (η is the resistivity), the helical flux ψ to aB_t, and the electron density n_e to its value at the magnetic axis, these equations become [18,41]

$$\frac{dn_e}{dt} = d_1\nabla_{||}j - \nabla_{||}(n_e v_{||}) + \nabla_\perp(D_{\perp N}\nabla_\perp n_e) + S_n, \tag{A1}$$

$$\frac{d\psi}{dt} = E_0 - \eta_N(j - j_b) - \frac{\eta_N}{\nu_{ei}}\frac{dj}{dt} + \Omega\left(\frac{T_e}{n_e}\nabla_{||}n_e + \nabla_{||}T_e\right), \tag{A2}$$

$$\frac{dU}{dt} = S^2\nabla_{||}j + \mu_N\nabla_\perp^2 U + S_m, \tag{A3}$$

$$\frac{dv_{||}}{dt} = -C_s^2\nabla_{||}P/n_e + \mu_N\nabla_\perp^2 v_{||}, \tag{A4}$$

where

$$\frac{d}{dt} = \frac{\partial}{\partial t} + \boldsymbol{v}_E\cdot\nabla_\perp, \tag{A5}$$

$$j = -\nabla_\perp^2\psi - 2nB_t/(mR) \tag{A6}$$

is the parallel plasma current density,

$$U = -\nabla_\perp^2\phi \tag{A7}$$

the plasma vorticity. $P = P_e = n_eT_e$ is the electron pressure,

$$j_b = -c_b\varepsilon^{0.5}(c_T n_e\partial T_e/\partial r + T_e\partial n_e/\partial r)/B_p \tag{A8}$$

is the bootstrap current density, c_b a constant of order of unity, $c_T = 0.367$, $\varepsilon = r/R$, B_p the poloidal magnetic field, T_e the electron temperature, and $\eta_N = 1$ the normalized resistivity. E_0 is the equilibrium electric field, S_n the particle source, and S_m the poloidal momentum source leading to an equilibrium poloidal plasma rotation. $\Omega = \beta d_1$, $d_1 = \omega_{ce}/\nu_{ei}$, $\beta = 4\pi P_e/B_t^2$, and ω_{ce} and ν_{ei} are the electron cyclotron and the electron-ion collisional frequency. $S = \tau_R/\tau_A$, where $\tau_A = a/V_A$ is the Alfven time, and V_A is the Alfven velocity defined using the toroidal field. C_s, μ_N and $D_{\perp N}$ are the normalized ion sound velocity, plasma viscosity, and perpendicular particle diffusivity.

The cold ion assumption is made. The third term on the right hand side of equation (A2), being proportional to $1/\nu_{ei}$, takes into account the electron inertia. When solving equations (A1)-(A4)

alone, a constant electron temperature is assumed.

For the *low resistivity case*, the input parameters are based on medium size tokamak experimental parameters: $T_e = 2keV$, $n_e = 3 \times 10^{19} m^{-3}$, $a = 0.5m$, $R = 1.7m$, and $B_t = 2T$, leading to $S = 2.6 \times 10^8$, $C_s = 2 \times 10^7\ (a/\tau_R)$, $\eta_N = 1$, and $d_1 = 3.1 \times 10^7$. The perpendicular plasma momentum and particle transport are assumed to be at an anomalous transport level of $\mu = 0.2m^2/s = 18.8a^2/\tau_R$ and $D_\perp = \mu/5$.

For the *high resistivity case*, the following input parameters are used: $T_e = 300eV$, $n_e = 10^{19} m^{-3}$, $a = 0.25m$, $R = 1m$, and $B_t = 2T$, leading to $S = 3.76 \times 10^7$, $C_s = 8.4 \times 10^5\ (a/\tau_R)$, $d_1 = 5.4 \times 10^6$, and $\Omega = 8.2 \times 10^2$. Furthermore, $f_b = m_e = 0$ and $\mu = D_\perp = 0.2m^2/s$ are assumed.

For the results in Section 3.4, the electron heat transport equation [21]

$$\frac{3}{2} n_e \frac{dT_e}{dt} = d_1 T_e \nabla_{||} j - T_e n_e \nabla_{||} v_{||} + n_e \nabla \cdot (\chi_{||} \nabla_{||} T_e) + n_e \nabla \cdot (\chi_\perp \nabla_\perp T_e) + S_p, \qquad \text{(A9)}$$

is solved together with equations (A1)-(A4), to take into account the electron temperature perturbations, where χ the heat conductivity, and S_p is the heat source. The ratio between the parallel and perpendicular heat conductivity, $\chi_\parallel/\chi_\perp = 10^9$, $\chi_\perp = \mu$ and a parabolic profile for the equilibrium electron temperature are assumed.

The tokamak plasma rotation in the core region is essentially toroidal, while only the poloidal rotation is included in equations (A1)-(A4) due to the large aspect ratio approximation. To guarantee a reasonable balance between the electromagnetic (EM) and viscous force, a larger plasma viscosity for the $m/n = 0/0$ component (by a factor 10^2) is used in (A3) based on the following considerations [4]: (a) The EM force in the toroidal direction is smaller by a factor $(n/m)(r_s/R)$ than that in the poloidal direction. (b) To have the same mode frequency due to the plasma rotation, the toroidal rotation velocity should be $(m/n)(R/r_s)$ times larger than the poloidal one. These two effects lead to a larger viscous force compared to the EM force for the toroidal rotation case by a factor $[(m/n)(R/r_s)]^2 \sim 10^2$.

Appendix B Electron fluid velocity and tearing mode frequency

The electron diamagnetic drift velocity is

$$\boldsymbol{v}_{*\boldsymbol{e}} = \nabla P_e \times \boldsymbol{B}/(n_e|e|B^2), \qquad \text{(B1)}$$

which is mostly in the poloidal direction with a poloidal component

$$\boldsymbol{v}_{*e,p} \approx v_{*e,p} \boldsymbol{e}_p, \qquad \text{(B2)}$$

where $v_{*e,p} = -P'_{e,N} B_t/B^2$, $P'_{e,N} = P'_e/(n_e|e|)$, and e is the electron charge.

The electric drift velocity is

$$\boldsymbol{v}_E = \boldsymbol{E}_r \times \boldsymbol{B}/B^2, \tag{B3}$$

where $\boldsymbol{E}_r = E_r \boldsymbol{e}_r$ is the radial electric field.

When there is no poloidal rotation damping, the electric drift is dominated by its poloidal component,

$$\boldsymbol{v}_{E,p} = v_{E,p} \boldsymbol{e}_p, \tag{B4}$$

where $v_{E,p} = -E_r B_t/B^2$**.** In this case the bi-normal electron fluid velocity is found from (B2) and (B4),

$$\boldsymbol{v}_{\boldsymbol{e}} = \boldsymbol{v}_E + \boldsymbol{v}_{*e} = -[(E_r + P'_{e,N})B_t \boldsymbol{e}_p]/B^2. \tag{B5}$$

The angular frequency of the tearing mode is determined by the local bi-normal electron fluid velocity at the resonant surface [41],

$$\omega_{e\perp} = (\omega_{E0} + \omega_{*e0}) = \boldsymbol{k} \cdot \boldsymbol{v}_{\boldsymbol{e}} = -\left(\frac{m}{r}\right)(E_r + P'_{e,N})B_t/B^2, \tag{B6}$$

where $\boldsymbol{k} = m\boldsymbol{e}_p/r + n\boldsymbol{e}_t/R$. (B5) and (B6) show that if $E_r > -P'_{e,N}$, $\omega_n < 0$, and the electron fluid velocity is in the ion drift direction.

When the poloidal electric drift is negligible due to neoclassical damping, which is usually the case for tokamak core plasmas, the toroidal electric drift velocity is

$$\boldsymbol{v}_{E,t} = v_{E,t} \boldsymbol{e}_t, \tag{B7}$$

where $v_{E,t} = E_r B_p/B^2$**.** In this case the electron fluid velocity is found from (B2) and (B7),

$$\boldsymbol{v}_e = \boldsymbol{v}_E + \boldsymbol{v}_{*e} = [E_r B_p \boldsymbol{e}_t - P'_{e,N} B_t \boldsymbol{e}_p]/B^2, \tag{B8}$$

and the angular mode frequency

$$\omega_{e\perp} = \left(\frac{m}{r}\right) v_{*e,p} + \left(\frac{n}{R}\right) v_{E,t} = [-\left(\frac{m}{r}\right) P'_{e,N} B_t + \left(\frac{n}{R}\right) E_r B_p]/B^2. \tag{B9}$$

The parallel wave vector is zero at the resonant surface for the tearing mode, i.e.

$$\boldsymbol{k} \cdot \boldsymbol{B} = \left(\frac{m}{r}\right) B_p + \left(\frac{n}{R}\right) B_t = 0, \tag{B10}$$

which leads to $q = q_s$ at the resonant surface, where $q = rB_t/(RB_p)$ and $q_s = -m/n$. Therefore, (B9) can be written in the form

$$\omega_{e\perp} = \omega_{*e0} + \omega_{E0} = \left(\frac{nB_p}{RB^2}\right)\left[\left(\frac{q_s^2 R^2}{r^2}\right) P'_{e,N} + E_r\right]. \tag{B11}$$

where $\omega_{*e0} = nP'_{e,N}/(B_p R)$ and $\omega_{E0} = nB_p E_r/(RB^2)$. It is seen from (B11) that for $E_r > 0$, the contribution of the electric and the electron diamagnetic drifts to the frequency has the opposite sign.

Using (B7), equation (B11) can be written in another form

$$\omega_{e\perp} = \left(\frac{nB_p}{RB^2}\right)\left[\left(\frac{q_s^2 R^2}{r^2}\right) P'_{e,N} + B^2 v_{E,t}/B_p\right], \tag{B12}$$

which indicates that if $v_{E,t}/B_p > 0$ ($v_{E,t}$ in the plasma current direction), the contribution of the electric and the electron diamagnetic drifts to the frequency has the opposite sign, being independent

of the toroidal field direction. In this case, a negative value of ω_n corresponds to $B^2 v_{Et}/B_p > -P'_{e,N} q_s^2 R^2/r^2$, i.e. the toroidal electric drift is in the plasma current direction with a frequency being larger than the electron diamagnetic drift frequency. As described in Ref. [20], the electron diamagnetic drift frequency can also be written in another form, $\omega_{*e0} = \mathrm{v}_{*\mathrm{e,t}}\mathrm{n/R}$, with a toroidal drift velocity $\mathrm{v}_{*\mathrm{e,t}} = \mathrm{P}'_{\mathrm{e,N}}/\mathrm{B}_{\mathrm{p}}$ in the counter current direction. This is equivalent to the ω_{*e0} calculated from the poloidal diamagnetic drift velocity by making use of equation (B10).